energies

MDPI

Article

Development and Evaluation of Velocity Predictive Optimal Energy Management Strategies in Intelligent and Connected Hybrid Electric Vehicles

Aaron Rabinowitz [1], Farhang Motallebi Araghi [2], Tushar Gaikwad [2], Zachary D. Asher [2,*] and Thomas H. Bradley [1]

[1] Department of Systems Engineering, Colorado State University, Fort Collins, CO 80523, USA; aaron.rabinowitz@colostate.edu (A.R.); Thomas.Bradley@colostate.edu (T.H.B.)
[2] Department of Mechanical and Aerospace Engineering, Western Michigan University, Kalamazoo, MI 49008, USA; farhang.motallebiaraghi@wmich.edu (F.M.A.); tushar.gaikwad@wmich.edu (T.G.)
* Correspondence: zach.asher@wmich.edu

Abstract: In this study, a thorough and definitive evaluation of Predictive Optimal Energy Management Strategy (POEMS) applications in connected vehicles using 10 to 20 s predicted velocity is conducted for a Hybrid Electric Vehicle (HEV). The presented methodology includes synchronous datasets gathered in Fort Collins, Colorado using a test vehicle equipped with sensors to measure ego vehicle position and motion and that of surrounding objects as well as receive Infrastructure to Vehicle (I2V) information. These datasets are utilized to compare the effect of different signal categories on prediction fidelity for different prediction horizons within a POEMS framework. Multiple artificial intelligence (AI) and machine learning (ML) algorithms use the collected data to output future vehicle velocity prediction models. The effects of different combinations of signals and different models on prediction fidelity in various prediction windows are explored. All of these combinations are ultimately addressed where the rubber meets the road: fuel economy (FE) enabled from POEMS. FE optimization is performed using Model Predictive Control (MPC) with a Dynamic Programming (DP) optimizer. FE improvements from MPC control at various prediction time horizons are compared to that of full-cycle DP. All FE results are determined using high-fidelity simulations of an Autonomie 2010 Toyota Prius model. The full-cycle DP POEMS provides the theoretical upper limit on fuel economy (FE) improvement achievable with POEMS but is not currently practical for real-world implementation. Perfect prediction MPC (PP-MPC) represents the upper limit of FE improvement practically achievable with POEMS. Real-Prediction MPC (RP-MPC) can provide nearly equivalent FE improvement when used with high-fidelity predictions. Constant-Velocity MPC (CV-MPC) uses a constant speed prediction and serves as a "null" POEMS. Results showed that RP-MPC, enabled by high-fidelity ego future speed prediction, led to significant FE improvement over baseline nearly matching that of PP-MPC.

Keywords: HEV; V2X; fuel economy; Dynamic Programming; MPC; ANN; LSTM; systems engineering

Citation: Rabinowitz, A.; Motallebi Aaraghi, F.; Gaikwad T.; Asher, Z.D.; Bradley, T.H. Development and Evaluation of Velocity Predictive Optimal Energy Management Strategies in Intelligent and Connected Hybrid Electric Vehicles. *Energies* **2021**, *14*, 5713. https://doi.org/10.3390/en14185713

Academic Editor: Mario Marchesoni

Received: 20 July 2021
Accepted: 7 September 2021
Published: 10 September 2021

1. Introduction

Improving FE is a critical goal to reducing climate change and air pollution. The transportation sector is responsible for 27% of all greenhouse gas emissions produced globally and more than 50% of nitrogen oxide emissions [1]. Recent studies show that greenhouse gas emissions are a significant contributor to global climate change [2] and lowered life expectancy in many countries [3]. Greenhouse gas emission levels are directly related to the FE of vehicles; reducing total miles driven is a difficult-to-implement and politically controversial goal, thus much research into methods to improve vehicle fuel economy (FE) has been performed [4].

A critical component of improving FE is vehicle electrification. Recently, Hybrid Electric Vehicles (HEV) and Plug-in Hybrid Electric Vehicles (PHEV) have been widely researched because of their greater potential to increase fuel economy (FE) and emissions over that of conventional Internal Combustion Engine (ICE) vehicles [5]. However, currently available HEVs do not operate optimally [6].

In addition to advancements in powertrain technology, recent developments in the automotive industry have led to huge advancements in Intelligent and Connected Vehicle (ICV) technology. Advanced Driver Assistance System (ADAS) technology has seen rapid market penetration due to its potential to bring safety and convenience benefits to customers [7–9]. Automation (i.e., ADAS) and connectivity (i.e., ICV) technology are critical technologies not only for safety and commercialization of autonomous vehicles but also for energy efficiency through implementation of Predictive Optimal Energy Management Strategies (POEMSs) on HEVs and PHEVs which can increase their FE and reduce their emissions [10–14].

POEMSs use predicted vehicle velocity (enabled through ADAS [15] and connectivity) as an input to optimal control. The optimal solution output is then used as an input to the vehicle plant, ideally an HEV or PHEV due to the additional operational degrees of freedom [16]. This process has been the subject of active research since the first publication in 2001 [10]. Note that in the current transportation environment, perfect future velocity prediction is not possible. To address this issue, researchers have used Model Predictive Control (MPC) which, in this context, is the application of DP optimization to fixed length prediction windows. Research in this space has demonstrated that perfect velocity prediction is not required [17], and that even heuristic approaches which rely on acceleration event prediction can be used [12,18] to achieve improvements in FE. However, it is worth noting that these FE improvements are modest compared to those theoretically achievable with prefect prediction of vehicle velocity. High-fidelity prediction of future vehicle velocity is presently achievable through the employment of machine learning (ML) and Artificial Neural Network (ANN) methods and ICV technology [19–26]. Despite all of this research, a thorough investigation of the datasets and prediction models' effect on vehicle FE (the full system) has not been conducted. The latest research has explored the effect on velocity prediction error metrics rather than resultant vehicle FE [26,27]. In order to facilitate real-world implementation, certain specific research gaps must be addressed; these research gaps are defined in [16] as:

1. Performance of Optimal EMS with Actual Velocity Predictions;
2. Performance of Optimal EMS when Subjected to Disturbances;
3. Performance of Optimal EMS in Real Vehicles.

To the author's knowledge, this paper represents the first comprehensive study fully addressing Research Gap 1. Previous research in the area of POEMS has focused on select aspects of Research Gap 1 but no comprehensive study has been performed which concerns the use of real-world data and real-time prediction methods in POEMS. This study, being such a comprehensive analysis, allows for research to progress towards other aspects of implementation namely Research Gaps 2 and 3. Previous research in this area is summarized as follows. The efficacy of predictive Optimal EMS for improving efficiency in HEVs was first shown in 2001 in [10] utilizing perfect prediction. In 2008, velocity prediction was introduced to the literature in [28] which used an analytical traffic based velocity prediction model. In 2015, the advantages of ANN prediction were shown in [21,22]. In 2017 and 2018, a series of studies [15,17,29,30] experimented with different data streams to optimize prediction with a shallow ANN. In 2019, more modern machine learning techniques were introduced into the field in [31] where reinforcement learning was used along with traffic data to train an ANN to produce optimal controls for a power-split hybrid. Also in 2019, Refs.[26,32] showed that high-fidelity predictions were possible through the use of deep Long Short-Term-Memory (LSTM) ANNs. Finally, in 2020, a thorough analysis of various combinations of real-world data streams and machine learning techniques [26,27,33]

showed that the highest degree of prediction fidelity could be attained through the use of LSTM ANNs with the use of signal phase and timing (SPaT) and lead vehicle data.

Thus, in order to close the gap, this paper outlines a comprehensive system-level study addressing the interactions between groups of available real-world data, velocity prediction methods, and Optimal EMS methods with respect to the overall system output: FE.

This paper rigorously evaluates the dataset and perception model for POEMS and evaluates performance using the FE for a validated HEV to enable full system performance insight, which to-date is missing from the literature. Cutting-edge AI technology is leveraged to generate high-fidelity future vehicle velocity predictions in 10 to 20 s windows. The predictions are fed into an MPC control method in order to determine the optimal instantaneous torque split for a power-split HEV. The FE achievable with the proposed POEMS will be compared to that achievable with perfect prediction full-drive-cycle DP (FCDP), perfect prediction MPC (PP-MPC), constant velocity-prediction MPC (CV-MPC), and Autonomie baseline control. This paper will further show that the proposed method is implementable on current vehicles with current technology and has the potential to provide significant FE improvements within the HEV fleet if implemented.

2. POEMS Methodology

2.1. Overall System

HEV POEMS uses predictions of future vehicle velocity to inform an optimal power-train control strategy, thus achieving greater energy efficiency. Powertrain controls include torque split and gear shifting based on powertrain states such as battery State of Charge (SOC) and current gear in the case of a parallel power-train configuration or only torque split in the case of a parawhnllel configuration.

As shown in Figure 1, a POEMS consists of three major subsystems. The first is the perception system which predicts vehicle motion using information about previous and current vehicle motion, powertrain states, driver inputs,eh ADAS, and V2X data as inputs. The second is the planning subsystem which computes optimal controls based on the predicted vehicle velocity. Finally, the third subsystem is the vehicle plant which can be either the physical vehicle or high-fidelity simulation model of the vehicle. The final system outputs are the actual vehicle velocity and powertrain states.

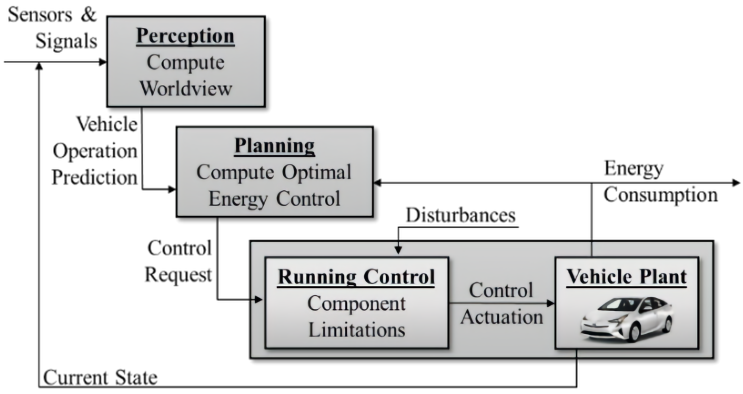

Figure 1. POEMS logic flow schematic.

POEMS achieve greater FE by ensuring that the engine is used in regions of maximum efficiency as often as possible. This concept is shown in Figure 2 which includes a Brake-Specific Fuel Consumption (BSFC) map for an example engine and different combinations of engine speed and torque which produce different engine efficiencies. Thus, most engine controllers attempt to operate the engine along its Ideal Operating Line (IOL) [34] which contains the most efficient torque for a given engine speed. POEMS use information about future vehicle velocity to ensure that the engine only operates in the most efficient segment of the IOL, what can be thought of as an Ideal Operating Line Segment (IOLS).

As shown in Figure 2, simply operating along the IOL (yellow dots) does not guarantee efficient operation. POEMSs increase FE by guaranteeing operation within the IOLS (green dots).

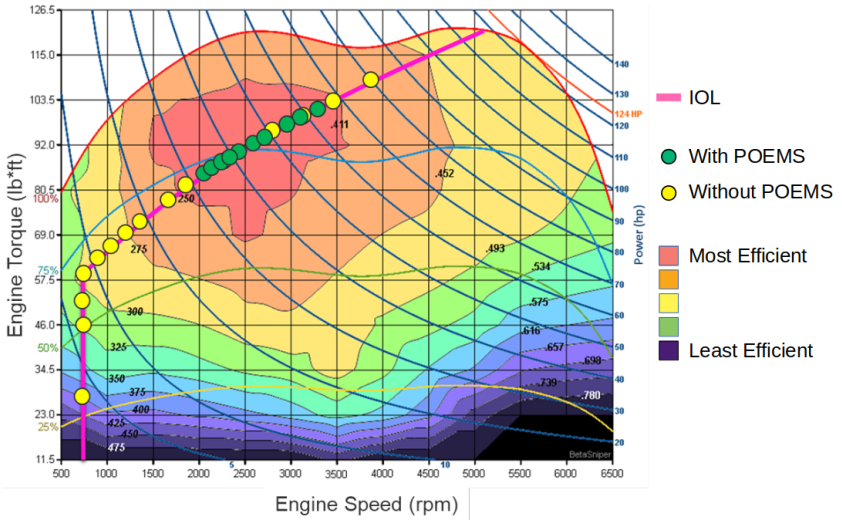

Figure 2. Example BSFC plot with IOL and operating points with and without POEMS.

Although this paper only concerns vehicle motion, the POEMS method can be extended to account for additional exogenous inputs such as cabin heating and cooling requirements [35–37] without fundamentally changing the method.

2.2. System Inputs

2.2.1. Dataset Development

The first step in the development of practical and high-fidelity real-world future vehicle speed prediction was to collect a sample generic dataset which would represent all data sources potentially available to a given ICV. All data sources selected are currently available to ICVs or will be available in the near future [38]. In this section, a taxonomy for such a dataset is defined. This taxonomy defines data both in terms of source form and processed form and defines the process of transformation.eh

The first step in defining the dataset is to define the sources of the data. Three distinct source categories are proposed:

1. VEH: Vehicle operational data such as vehicle motion, performance, and driver inputs. These data only concern the ego vehicle itself and its driver.
2. ADAS: Advanced Driver Assistance System (ADAS) data [39]. This consists of the data generated by external object sensors on the vehicle and concerns objects within the vehicle's line of sight.
3. V2I: Data which the vehicle receives through connectivity to infrastructure and other vehicles.

In order to be considered an ICV, a vehicle must receive information from all three of the above sources. Most modern vehicles receive data from the VEH and ADAS sources [40] and V2I is available in some regions [41]. These signals were obtained from the ego vehicle CAN bus and the City of Fort Collins, Colorado.

Within these source categories, signals of use in vehicle future velocity prediction are shown in Table 1.

All VEH signals should be available on all modern vehicle CAN networks while ADAS-enabled vehicles will produce a lead vehicle track for safety and Autonomous Cruise Control (ACC) purposes. The information for SPaT and SS comes form the SAE J2735 SPaT/Map message. Thus, all signals used in this study are available to a generic ICV while traveling on a connected infrastructure. Most modern vehicles will have access to

the VEH and ADAS sourced signals. A total of 13 drive cycles worth of data were collected along the data drive cycle by one driver over two days. Details about data collection and availability can be found in the team's previous work [33].

Table 1. Data sources and associated signals.

Data Source	Signal	Description
VEH	General Vehicle Signals	Signals such as speed, acceleration, throttle position, and steered angle which can be found via CAN on any vehicle
VEH	Historical Speeds (HS)	Historical speed data for the vehicle at the current location
ADAS	Lead Vehicle Track (LV)	Relative location of confirmed lead vehicle from ADAS system
V2I	Signal Phase and Timing (SPaT)	Signal phase and timing of next traffic signal
V2I	Segment Speed (SS)	Traffic speed through current road segment

2.2.2. Data Drive Cycle Selection

In order to gauge the effects of real-world data-based predictions on the performance of POEMS, a real-world dataset was required. It was desired to gather data in conditions which would allow for optimal POEMS performance such that the relative differences between various POEMS methods would be as great as possible. A secondary consideration was that, in order to allow for optimal ML and ANN prediction performance, the data collection should be conducted along a repeating drive cycle and that this cycle should be short enough that more than 10 cycles could be collected in a single day. The drive cycle which was selected was a 4 mile long drive cycle along urban arterial roads in downtown Fort Collins, Colorado which is shown in Figure 3.

Figure 3. Selected data drive cycle; drive order was purple, yellow, blue, then green, red circles represent traffic signals

In order to assess the characteristics of the data drive cycle, it was determined that the data drive cycle and the EPA dynamometer drive cycles should be characterized by their distributions of speeds and accelerations. These basic statistical measures were chosen in order to allow for easy comparison between the drive cycles. The drive cycle characteristics data are shown in Table 2.

Table 2. Drive cycle characteristics for data drive cycle and EPA drive cycles

Drive Cycle	Mean Non-Zero Speed (MNZS)	Standard Deviation of Non-Zero Speeds (SNZS)	Mean Absolute Acceleration (MAA)	Standard Deviation of Absolute Accelerations (SAA)
Data	18.6988	8.5699	1.1557	1.1432
UDDS	10.7923	5.5850	0.4723	0.4859
US06	23.1791	9.5014	0.6538	0.7851
HWFET	21.7191	4.1752	0.1713	0.2443

Based on these characteristics, the similarity of the data drive cycle and the EPA dynamometer drive cycles was calculated using the multivariate normal distribution. The relative similarities between the EPA cycles and the data drive cycle are shown in Table 3.

Table 3. Relative similarities between EPA dynamometer drive cycles and the data drive cycle.

UDDS	US06	HWFET
0.5885	0.2394	0.1721

It must be stressed that the comparison between a data drive cycle and the EPA dynamometer drive cycles could only be calculated after data collection was performed and the data drive cycle was known. Of the candidate data drive cycles tried, the drive cycle shown in Figure 3 resulted in the most favorable comparison to EPA dynamometer drive cycles.

The selected data drive cycle was most similar to the UDDS EPA dynamometer drive cycle because higher numbers imply that the real-world drive cycle from Figure 3 is more similar.

2.3. Subsystem 1: Perception

Having collected an extensive real-world ICV dataset, a comprehensive study on prediction methods was conducted. The initial analysis of the prediction study can be found in [26] and is summarized below:

A wide field of potential prediction algorithms including classical ML and ANN methods were considered. The candidate methods are listed in Table 4.

All methods were trained, tested, and validated on a 9/2/2 data-split basis, respectively. The training and evaluation metric was Mean Absolute Error (MAE), where X is the predicted velocity value, Y is the actual velocity value, and n is the total number of timesteps.

$$MAE(X,Y) = \frac{\sum_{i=1}^{n} |X_i - Y_i|}{n} \quad (1)$$

An extensive study was conducted on different combinations of the signals in Table 1 as well as different combinations of macro-parameters for the methods. From this general study, the best results for each method for 10, 15, and 30 s time horizon speed predictions in terms of MAE are listed in Table 5.

The results of the general study showed that the LSTM had the best performance at 10, 15, and 20 s.

Based on this collected evidence, it was concluded that an LSTM should be used within the POEMS system. For further discussions and details, the reader is referred to the team's previous publications [26,27].

Table 4. Candidate Prediction Methods.

Method	Method Type
Long Short Term Memory (LSTM) Deep Neural Network (DNN)	ANN
Convolutional Neural Network (CNN)	ANN
CNN-LSTM	ANN
Decision Trees	ML
Bagged Trees	ML
Random Forest	ML
Extra Trees	ML
Ridge	ML
K-Nearest-Neighbors (KNN)	ML
Linear Regression without Interactions (LR)	Statistical
Linear Regression with Interactions (LRI)	Statistical

Table 5. The candidate prediction methods results organized from best performing to worst performing.

Method	MAE—10 s	MAE—15 s	MAE—20 s
LSTM	1.78	2.55	3.09
CNN	1.84	2.77	3.50
CNN-LSTM	1.97	2.7	3.26
Decision Trees	2.69	3.60	4.12
Bagged Trees	2.23	3.09	3.67
Random Forest	2.30	3.15	3.72
Extra Trees	1.99	2.73	3.30
Ridge	2.67	3.84	4.67
KNN	2.67	3.84	4.67
LR	2.65	3.82	4.65
LRI	2.57	3.60	4.28

2.4. Subsystem 2: Planning

HEV POEMS planning subsystems generally fall into two groups: (1) those based on Pontryagin's Maximum Principle (PMP) such as ECMS [42], a-ECMS [11], as well as their derivatives, and (2) those based on DP. The advantages of PMP methods is that these are "real-time" strategies since they are relatively computationally cheap. However, this method is typically non-optimal and recent research suggests that the equivalence factor

prediction is analogous to velocity prediction [43]. The advantages of DP based methods is that they guarantee discovery of the globally optimal solutions assuming that the vehicle velocity prediction is accurate. The research team discovered the critical importance of this aspect through documenting that even if significant and real-world velocity mispredictions are present, the solution is still near optimal [44] which has lead to new method of real-world practical implementation [12,18]. Additionally, the rise in the use of AI within the CAV space has led to deployments of vehicles with high-performance GPUs on-board the vehicle which potentially enables real-time computation of DP [45], which has been a common criticism for eventual DP implementation. For these reasons, DP methods were selected for this study.

DP is a numerical method based on Bellman's principle of Optimality, which solves multistage decision-making problems and finds the global optimal solution by operating recursively backwards through time and storing only the optimal controls at each step [46,47]. DP and its derivative strategies have been applied to the problem of FE optimization for HEVs previously [6,10,48,49] for full and partial drive cycles as well as for perfect and real predictions.

DP can be thought of as a recursive equation solver with memory. A recursive solution to a problem is to evaluate all possible paths by evaluating every possible combination of decisions independently. While a recursive solution will find a global optimum, it will require an exponentially increasing number of function evaluations for each additional time-step. DP solves this run-time problem by iterating backwards through time and storing the optimal controls for each discreet state value at each time-step then evaluating the same controls from the same discreet state values until the first time-step. The result of the backward iteration is an optimal control matrix which can be used to find optimal controls at each time-step based on the current state values when iterating forwards. The backwards iteration step is referred to as the optimization step while the forward iteration step is referred to as the evaluation step. The DP method is shown schematically in Figure 4.

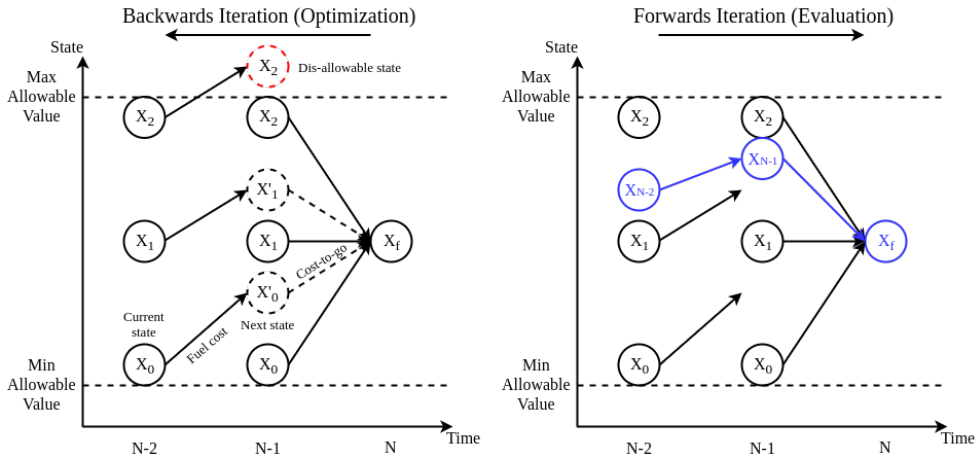

Figure 4. Schematic of DP method.

The optimization step of the DP method, as shown in Figure 4, creates an optimal matrix which can be used to compute optimal controls at each step by combining current and "remembered" costs. The optimization step iterates backwards from the last time-step (N) to the first which is not shown. The state values (represented by solid-outlined circles) show discreet state values. At time-step N-1, the model is evaluated for each of the discreet state values at each discreet control value which results in a series of new "intermediate" state values (represented by dashed-outlined circles) and associated control costs. Following this, the lowest cost (optimal) control is selected for each discreet state value. At time-step N-2 the same process is repeated but in addition to the control cost, the cost-to-go is calculated and added. The cost-to-go from a given intermediate state

value is calculated by interpolating from the stored optimal control costs from state N-1. This process repeats itself until the first time-step is reached. The DP method shown in Figure 4 is constrained in two ways: (1) a large penalty is applied for distance from the desired end state value at time-step N which forces the optimal controls for all state values at time-step N-1 to produce the same state value at time-step N and (2) controls which lead to intermediate states which are above or below the maximum and minimum value lines (represented by red dashed-outlined circles), respectively, are not considered. The output of the optimization step is an optimal control matrix which stores the optimal controls for each discreet starting state value at each time-step.

The evaluation step of the DP method, also shown in Figure 4, iterates forward from the first time-step through the last time-step from a given starting state value. At each time-step, interpolation is performed using the starting state value (represented by blue solid-outlined circles) and the optimal control matrix values for the current time-step to determine the optimal control for the current time-step. The optimal control is then applied and the starting state value for the subsequent time-step is calculated. This process is repeated until the penultimate time-step is reached.

2.4.1. High-Fidelity DP Solution for the HEV Optimization Problem

The formulation of the DP problem for the 2010 Toyota Prius is as follows:

- The powertrain state x is the battery SOC;
- The powertrain control u is the engine power;
- The exogenous input for the powertrain w is the vehicle speed;
- The time index k denotes the current time-step.

The general form of the dynamic equation is shown below. It uses a high-fidelity model of the vehicle to generate the SOC at time-step $k+1$ based on the SOC at time-step k, the engine power at time-step k, and the vehicle speed at time-step k as:

$$x(k+1) = x(k) + f(x(k), u(k), w(k))\Delta(t) \tag{2}$$

where $f(x(k), u(k), w(k))$ is the charging/discharging rate for the battery $dSOC/dt$. The charging/discharging rate function $f(x(k), u(k), w(k))$ can be written out as:

$$\frac{dSOC}{dt} = \frac{P_{batt}\epsilon_{chg}}{V_{oc}C} = \frac{(P_{batt,mot} + P_{batt,gen})\epsilon_{chg}}{V_{oc}C} \tag{3}$$

where V_{oc} and C are the battery open-circuit voltage and charge capacity, respectively. The charging/discharging efficiency is defined as:

$$\epsilon_{chg} = \begin{cases} C_{chg} & P_{batt} \geq 0 \\ C_{dchg} & P_{batt} < 0 \end{cases} \tag{4}$$

where C_{chg} and C_{dchg} are constants reflecting the battery's efficiency in charging and discharging, respectively. The powers $P_{batt,mot}$ and $P_{batt,gen}$ are calculated as follows:

$$P_{batt,mot} = \frac{T_{mot}\omega_{mot}}{\epsilon_{mot}} \tag{5}$$

$$P_{batt,gen} = \frac{T_{gen}\omega_{gen}}{\epsilon_{gen}} \tag{6}$$

The efficiencies ϵ_{mot} and ϵ_{gen} are the efficiencies of the motor and generator, respectively. Note that the efficiencies are in the denominator as the terms $P_{batt,mot}$ and $P_{batt,gen}$ are the power that the battery must provide to each to produce the required output powers $P_{mot} = T_{mot}\omega_{mot}$ and $P_{gen} = T_{gen}\omega_{gen}$ The following process is followed:

Starting with the current vehicle speed $w(k)$ and acceleration $\dot{w}(k)$ the vehicle power can be calculated using the road loads power equation.

$$P_{veh} = (m\dot{w}(k) + A + Bw(k) + Cw(k)^2)w(k) \tag{7}$$

where m is the vehicle mass and A, B, and C are vehicle-specific constants. For a given engine power u_i, the electric power required is:

$$P_{elec} = P_{veh} - u_i \tag{8}$$

For the given u_i, the engine torque and speed can be interpolated from the engine IOL and the combination of engine speed (ω_{eng}) and torque (T_{eng}) along with electric power can be used to determine the torques and speeds of the motor and generator from the planetary gearset dimensions.

The torques are calculated as follows:

$$T_{whl} = \frac{P_{veh}R_{whl}}{w(k)} \tag{9}$$

$$T_{pt} = \frac{T_{whl}}{\rho_{fd}} \tag{10}$$

$$T_{gen} = \frac{-\rho}{1+\rho}T_{eng} \tag{11}$$

$$T_{ring} = -\rho(T_{gen} - T_{eng}) \tag{12}$$

$$T_{mot} = T_{pt} - T_{ring} \tag{13}$$

where T_{whl} and R_{whl} are the torque applied at and the radius of the driven wheels, respectively, T_{pt} is the output torque of the power-train (before the differential) and ρ_{fd} is the final drive ratio, ρ is the gear ratio of the sun gear to the ring gear for the planetary gearset, T_{ring} is the torque of the ring gear, T_{gen} is the torque of the generator, T_{eng} is the torque of the engine, and T_{mot} is the torque of the motor.

And the speeds are calculated as follows:

$$\omega_{whl} = \frac{w(k)}{R_{whl}} \tag{14}$$

$$\omega_{mot} = \omega_{ring} = \rho_{fd}\omega_{whl} \tag{15}$$

$$\omega_{gen} = \frac{\rho+1}{\rho}\omega_{eng} - \frac{\omega_{ring}}{\rho} \tag{16}$$

where R_{whl}, R_{sun}, and R_{ring} are the radii of the wheel, sun gear, and ring gear, respectively, T_{pt} is the torque produced by the powertrain before the differential, and ρ_{fd} is the final drive ratio.

The cost function for the DP problem for control u_i at time-step k can be formulated as either a FE maximization or a fuel consumption minimization. Since fuel consumption minimization is more intuitive and widely used in previous studies, it will be utilized in this study.

$$J_i(k) = J_{im} + \begin{cases} J_{ctg} & k > N \\ J_{pen} = (x_f - x(k+1))^2 C_{pen} & k = N \end{cases} \tag{17}$$

where $J_{im,i}$ is the cost of fuel consumed to reach the intermediate state value which is calculated using the engine speed and torque and the engine FC map, J_{ctg} is the cost-to-go to the next state which is calculated through integration, and J_{pen} is the manually assigned penalty function associated with not arriving at the desired final *SOC* at the final time-step $k = N$.

2.4.2. Model Predictive Control (MPC) Methods

MPC is a framework to implement prediction-based optimal control. It utilizes a model of the system and a fixed time horizon to generate operational decisions. The DP model discussed in the previous section can be directly utilized in a fixed-horizon MPC framework with a few modifications.

The FCDP and a generic MPC methods are shown schematically in Figure 5.

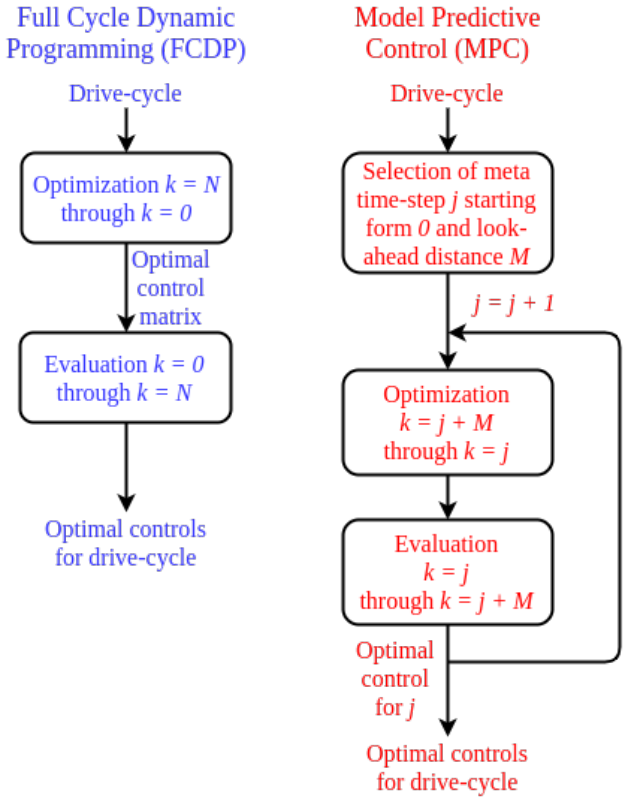

Figure 5. Schematic comparison between the FCDP and MPC methods.

In effect, MPC performs the DP method on a shortened drive cycle at each step of the actual drive cycle. Naturally, MPC should take significantly longer to run on a per time-step basis as full drive cycle DP. A more detailed explanation can be found in [26].

2.5. Subsystem 3: Vehicle Plant

This study was conducted using a validated Autonomie model of a 2010 Toyota Prius. The 2010 Prius is equipped with a Toyota e-CVT gearbox which utilizes two electric motors (motor and generator) connected to the engine and the differential through a planetary gearset to create a Continuously Variable Transmission (CVT) [50]. Because of the e-CVT architecture, the Prius driveline is controlled entirely by torque commands without having distinct gear states, thus the only powertrain control for the Prius is torque split and the only powertrain state is battery SOC.

Due to the lack of a publicly available FE model specific to the 2010 Toyota Prius, the model used was a generic Autonomie power-split HEV model which was modified to represent a 2010 Toyota Prius by setting the following parameters to the publicly available values shown in Table 6.

Validation of the Autonomie 2010 Prius model was conducted based on publicly available test results from Argonne National Laboratory's (ANL) Downloadable Dynamometer Database (D^3) [51]. The FE results obtained via the model for three EPA dynamometer drive cycles are compared to those found in D^3 in Table 7.

With all modeled FE values within 2% of those found in the ANL D^3 database, the Autonomie 2010 Toyota Prius model was considered validated for further research. It should be noted that, in accorance with physical testing procedure, the initial *SOC* for the vehicle model was set to fully charged for validation purposes but was set to 50% for furhter research. Thus, FE results for the same EPA dynamometer drive cycles later in the paper with baseline control will be slightly lower than those listed in Table 7.

Table 6. Parameters and values for the Autonomie 2010 Toyota Prius Model.

Parameter	Value
Overall Vehicle Mass	1530.87 kg
Frontal Area	2.6005 m^2
Coefficient of Drag	0.259
Coefficient of Rolling Resistance	0.008
Wheel Radius	0.317 m
Final Drive Ratio	3.267
Sun Gear Number of Teeth	30
Ring Gear Number of Teeth	78
Battery Open-Circuit Voltage	219.7 V
Battery Internal Resistance	0.373 Ω
Battery Charge Capacity	6.5 Ah

Table 7. EPA dynamometer drive cycle FE (km/L) results from the Autonomie 2010 Toyota Prius model and ANL D^3.

Drive Cycle	Data	Model	Percentage Difference
UDDS	32.14	31.79	1.09 %
US06	29.72	30.30	1.95 %
HWFET	19.26	18.98	1.45 %

2.6. System Outputs

In addition to FCDP and PP-MPC, the CV-MPC method was implemented. The CV-MPC method is functionally identical to PP-MPC except that the prediction vector is replaced with a speed vector where all speeds are the current vehicle speed. The CV-MPC method acts as a "null" predictive method which can serve as a point of comparison. The value of a given level of prediction fidelity can be gauged by its performance relative to PP-MPC and CV-MPC. A comparison of the DP-derived methods for a sample drive cycle is shown in Figure 6.

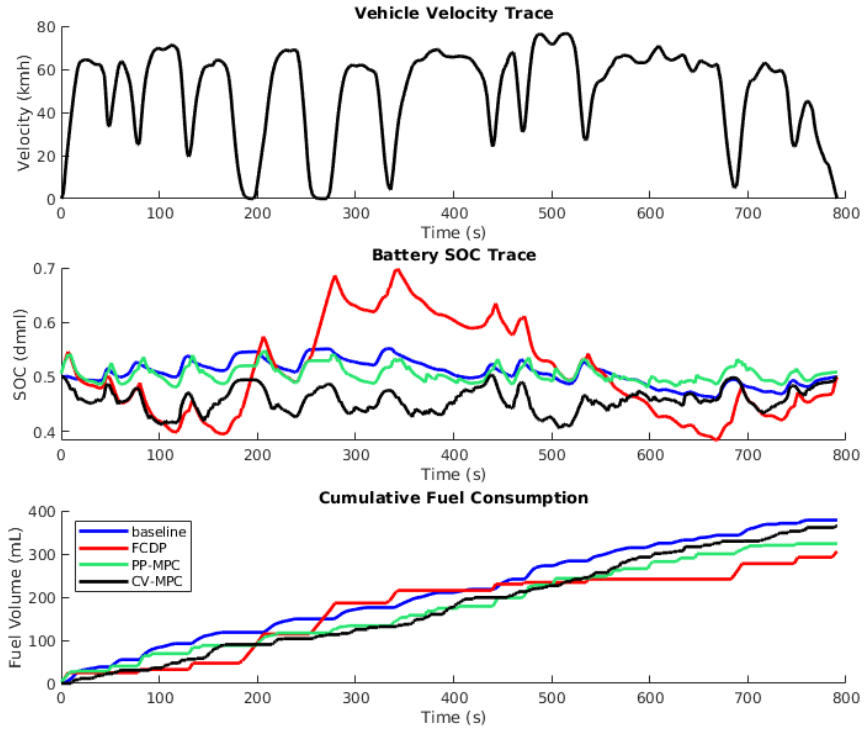

Figure 6. Comparison of DP-derived methods and Autonomie baseline control on sample drive cycle.

For the sample drive cycle in Figure 6, the FCDP method outperformed the PP-MPC method which outperformed the CV-MPC method and all outperformed the Autonomie baseline control method. Because of the double-sided charge-sustaining penalty, all SOC traces started and ended at exactly 50%, which means that fuel consumption can be compared directly without electrical equivalence. For the sample drive cycle, FCDP was able to outperform PP-MPC because it has more freedom to deviate from the start and finish SOC constraints. Generally, the longer the time horizon, the more effective PP-MPC should become. A study was conducted on the UDDS, US06, and HWFET EPA dynamometer drive cycles to demonstrate this. Results for the study are shown in Table 8.

Table 8. Fuel economy km/L for 2010 Toyota Prius model with DP-derived methods and Autonomie baseline on EPA dynamometer drive cycles (time horizon only effects the PP-MPC and CV-MPC methods).

Drive Cycle	Time Horizon	Baseline	FCDP	PP-MPC	CV-MPC
UDDS	10	28.28	40.32	39.11	35.10
UDDS	15	28.28	40.32	39.45	35.13
UDDS	20	28.28	40.32	39.71	35.00
US06	10	17.57	20.05	18.20	17.50
US06	15	17.57	20.05	18.44	17.20
US06	20	17.57	20.05	18.76	17.21
HWFET	10	28.13	28.59	26.30	24.24
HWFET	15	28.13	28.59	26.56	24.90
HWFET	20	28.13	28.59	26.64	24.37

An immediately noticeable trend is that increases in time horizon resulted in better FE for PP-MPC which allowed the PP-MPC FE to approach but not reach the FE produced by the FCDP method. Another noticeable effect is that the relative efficacy of the methods varied between the drive cycles with the DP-derived methods showing massive improvement over baseline in the stop-and-go UDDS drive cycle, while the PP-MPC and CV-MPC methods did not result in FE improvements for the relatively static HWFET drive cycle.

That DP-derived methods present the greatest potential for FE improvement in low-speed stop-and-go conditions is not a surprise. Low-speed stop-and-go conditions are where traditional control methods perform worst as they are unable to operate the IC engine in its most efficient areas. DP methods use knowledge of the future speeds of the vehicle to continue to operate the IC engine efficiently in stop-and-go conditions. An interesting result is that, even with inaccurate information about future vehicle velocity, the CV-MPC method significantly outperformed Autonomie baseline by a significant amount on the UDDS drive cycle.

3. Results

3.1. Direct Analysis of Velocity Prediction Accuracy using MAE

Based on the results of the general study documented in Section 2.3, a second, specific, study was carried out in order to optimize prediction fidelity from LSTM DNNs.

Long Short-Term Memory (LSTM) ANNs are a special case of Recurrent Neural Networks (RNNs) developed by Hochreiter and Schmidhuber [52] which utilize LSTM neurons in hidden layers. While classical recurrent neurons use a single gate to establish the relationship between inputs and outputs, LSTM neurons contain multiple gates which determine how much information should be remembered and forgotten within the neuron as well as the weighting of old and new information. The presence of the remember and forget gates allows LSTM neurons to utilize information from multiple time steps in the past [53,54]. For this reason, LSTM networks are ideally suited for problems where immediate and relayed reactions to inputs are present [55].

Because of its demonstrated feasibility, the LSTM is the prediction model which will be focused on. The following optimal architecture was arrived at:

The LSTM DNN described in Table 9 was selected for its high performance and reasonable training time. Adding more complexity to the network past the optimal network failed to generate significant performance gains. The LSTM DNN was trained on the groups of signals defined in Table 10.

Table 9. Structure of Optimal LSTM DNN.

Layer	Composition
1	Input layer-n_{inputs} fully connected
2	64 LSTM neurons
3	Dropout-10%
4	Batch normalization
5	32 LSTM neurons
6	12 LSTM neurons
7	Output layer-$n_{outputs}$ fully connected

Table 10. Data Groups for LSTM DNN.

Group Label	Composition
A	Speed, Acceleration, Engine Speed, Gear, Steered Angle, Throttle Position, Brake Pressure
B	A + HS + LV
C	A + HS + LV + SPaT + SS

The data groups were selected to reflect the data available to different categories of vehicle. A vehicle with neither ADAS nor connectivity only has access to A. Vehicles with ADAS and GPS navigation but no infrastructure connectivity have access to A and B. ICVs have access to all data groups. For groups A, B, and C a cross-validation study was run wherein the LSTM DNN was trained on 9 random laps, validated on 2 random laps, and tested on 2 random laps 30 times. The average MAEs for the cross-validation study are shown in Figure 7. The standard deviations of MAEs were all less than 5% of the mean values.

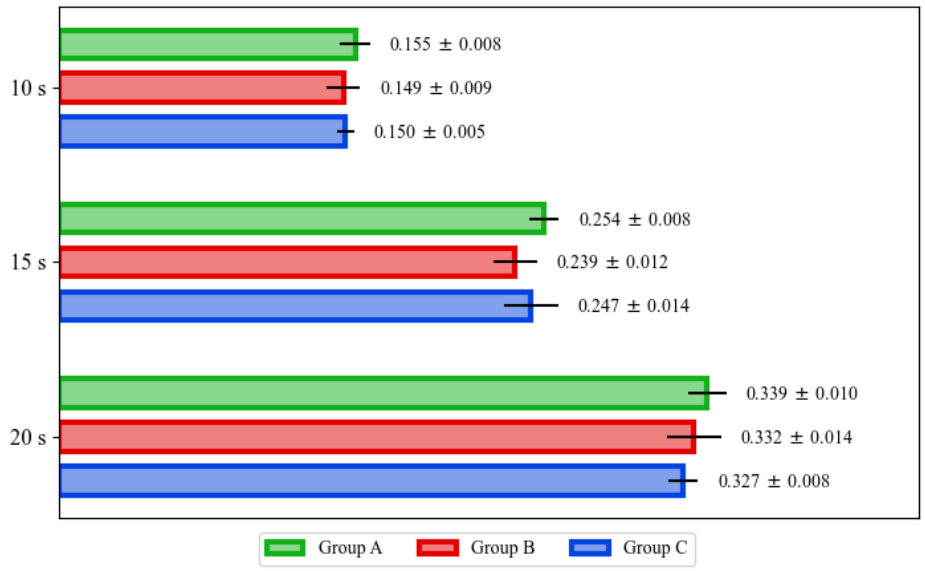

Figure 7. MAEs for LSTM DNN trained on data groups A, B, and C for 10, 15, and 20 s horizons.

As is evident in Figure 7, the difference in prediction performance between LSTM DNNs trained on the different data groups was minimal if slightly favoring group B over A and C. A visual comparison of the predictions for all groups at 10 and 20 s is shown in Figure 8.

As the prediction window increases, the LSTM DNN predictions are still able to rougly hold the shape of the velocity trace but produce a greater volume of mis-predictions. The predictions generated using LSTM DNNs trained on the different groups look slightly differently and produce slightly different MAEs but the time horizon length has, by far, the greater impact.

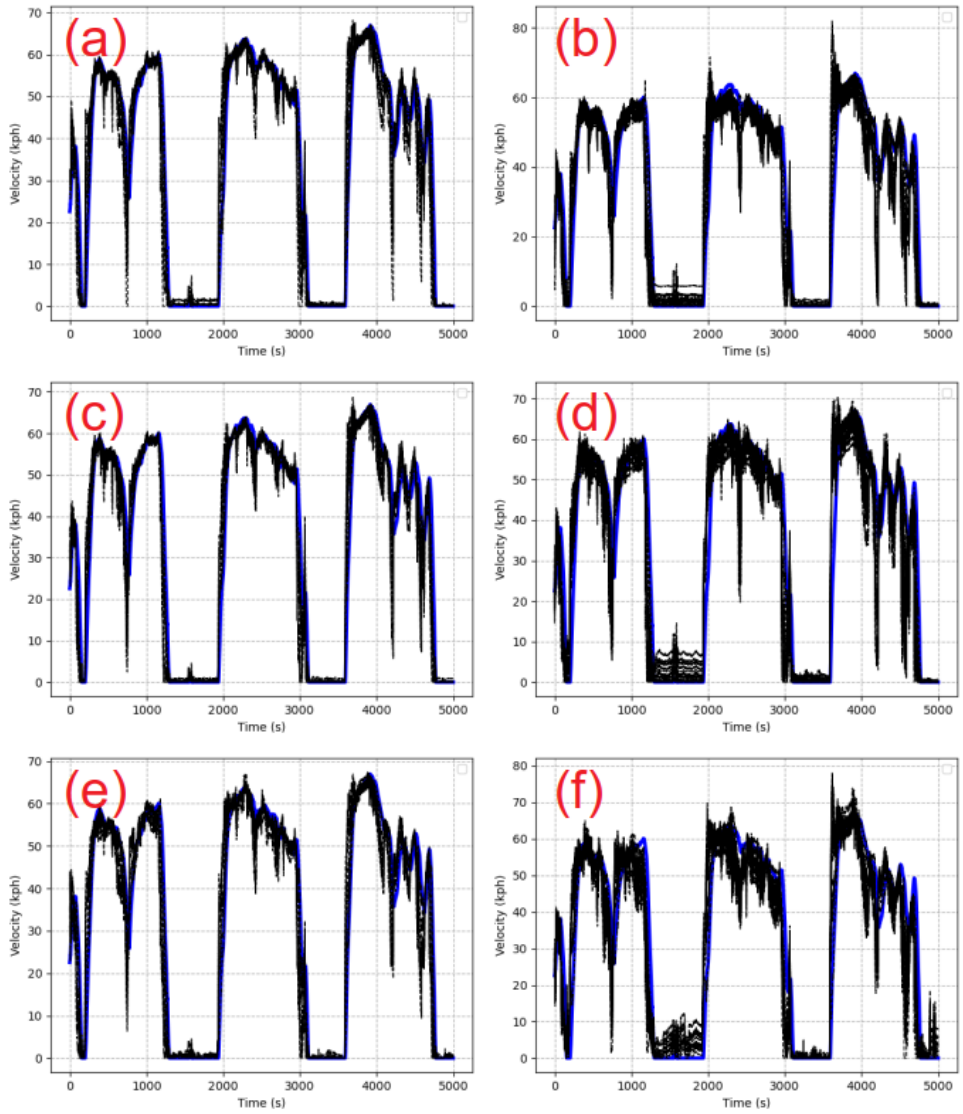

Figure 8. Predicted (black) vs. actual vehicle velocity (blue) for LSTM DNN trained on all data groups at 10 and 20 s prediction horizon. (**a**) is group A at 10 s, (**b**) is group A at 20 s, (**c**) is group B at 10 s, (**d**) is group B at 20 s, (**e**) is group C at 10 s, (**f**) is group C at 20 s.

3.2. Overall System FE Output

Using the predictions from the cross validation study mentioned in Section 3.1, FE simulations were conducted using the DP-derived methods and Autonomie baseline controls. The mean FE results for this study are listed in Table 11 and percentage improvements over baseline for the DP-derived methods with all data groups and at 10, 15, and 20 s are shown in Figure 9.

Table 11. FE (km/L) simulation results based on cross-validation study predictions.

Group Label	Prediction Horizon (s)	Baseline	FCDP	PP-MPC	RP-MPC	CV-MPC
A	10	18.33	24.10	21.78	20.73	20.07
B	10	18.33	24.10	21.78	20.85	20.07
C	10	18.33	24.10	21.78	20.83	20.07
A	15	18.33	24.10	21.87	21.24	20.01
B	15	18.33	24.10	21.87	20.45	20.01
C	15	18.33	24.10	21.87	20.15	20.01
A	20	18.33	24.10	22.22	20.80	20.00
B	20	18.33	24.10	22.22	20.75	20.00
C	20	18.33	24.10	22.22	21.05	20.00

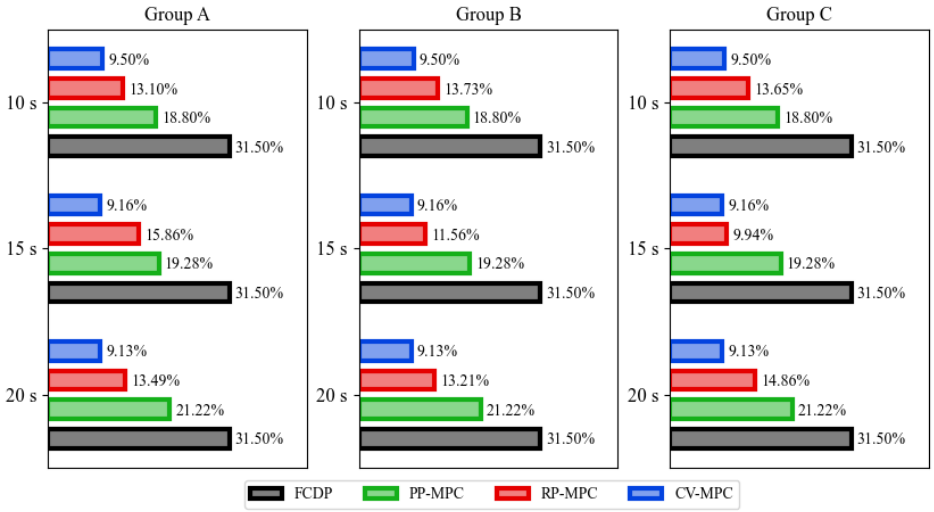

Figure 9. Percentage FE improvements for DP-derived methods for all data groups and time horizons.

3.3. Results Summary

The FE results for the DP-derived methods, when taken in conjunction with the results of the LSTM prediction illustrate several trends:

1. With perfect predictions MPC methods will produce better FE results for longer prediction horizons.
2. A greater volume of mis-predictions will result in worse FE results for MPC methods.
3. The small differences in prediction *MAE* observed between the data groups at all three time horizons are insufficient to explain the large differences observed in FE percentage improvement over baseline for the RP-MPC method between the data groups for the 15 and 20 s horizons.

It is illustrative that, for all cases, the average performance of the RP-MPC method came in between that of the CV-MPC and PP-MPC methods. The PP-MPC method, by definition, produces no mis-predictions while the CV-MPC method, by definition, produces only mis-predictions when the vehicle is moving. It would be logical for the RP-MPC method which produces some degree of mis-prediction to produce FE improvements which are somewhere between those produced by the CV-MPC and RP-MPC methods. The differences in vehicle future velocity prediction *MAE* between the data groups shown in Figure 7 were relatively small where the differences in FE improvement performance based on those predictions shown in Figure 9 were significant. Furthermore, no consistent

trend links the prediction MAE with the percentage FE improvement which leads to the conclusion that MAE is an insufficient metric to describe mis-prediction levels with respect to the RP-MPC method. Further research should be conducted to investigate whether other metrics serve better in this role.

The robustness of DP to velcity prediction error is directly demonstrated in the CV-MPC method which uses a "null" prediction of constant current speed over the entire prediction horizon. It showed significant improvements over baseline while the RP-MPC method showed significant improvements over CV-MPC. An examination of the data trace for all methods using predictions based on group A data for a 10 s prediction horizon are shown in Figure 10.

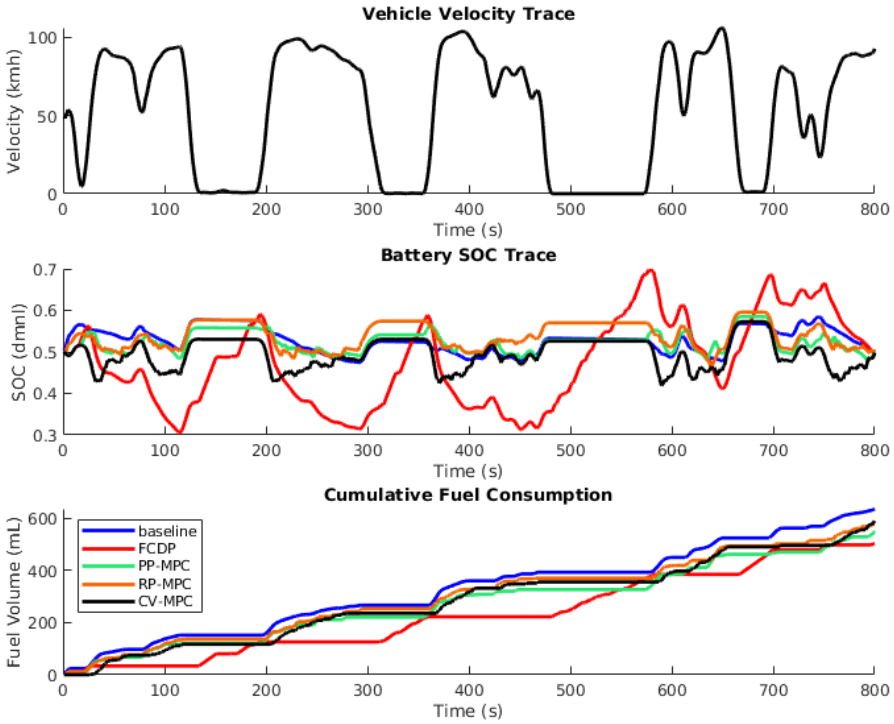

Figure 10. FE simulation data trace for all methods.

It can be clearly seen that the MPC methods discover similar local optima, and produce similar optimal state trajectories while the FCDP method, with much more freedom to deviate from the final SOC constraint, takes a substantially different path and ends up using less fuel.

4. Conclusions

In order to to demonstrate the function of various implementations, the data available to different types of vehicle were classified, an extensive real-world driving dataset was collected which incorporated said data, ML and ANN methods were used to predict the ego vehicle future speed using different groups of data, and the best predictions were used in FE simulation to determine the effectiveness of practically implementable POEMS. The results of the velocity prediction study showed that when using a LSTM DNN, high-fidelity velocity prediction was possible using only data which are available to conventional vehicles without ADAS or V2X connectivity and that the addition of ADAS and V2X connectivity resulted in modest fidelity gains. The results of the FE study showed the following:

- FE improvement achievable with RP-MPC approaches and with PP-MPC.
- RP-MPC consistently outperformed CV-MPC.

- Predictions made with ADAS and V2X resulted in greater FE improvement in the 20 s window.

An unavoidable conclusion is that the relationship between prediction fidelity and FE improvement using DP-derived methods cannot be explained by differences in prediction MAE.

This study shows that POEMS implementation on HEVs and PHEVs is feasible with causal and implementable prediction and control technologies and would lead to significant improvements in HEV and PHEV fleet efficiency if implemented. The same system architecture as autonomous vehicles (perception, planning, control, plant) can be applied to energy efficiency through the deployment of POEMS-enabled vehicles. The FE improvement which would result is significant and the technology can be implemented currently. The results of this study thus serve as a step towards real-world implementation and commercialization.

Author Contributions: Conceptualization, A.R.; Formal analysis, A.R.; Funding acquisition, Z.D.A. and T.H.B.; Investigation, A.R., F.M.A. and T.G.; Methodology, A.R. and T.G.; Project administration, Z.D.A. and T.H.B.; Software, A.R.; Supervision, Z.D.A. and T.H.B.; Writing—original draft, A.R.; Writing—review & editing, A.R., Z.D.A. and T.H.B. All authors have read and agreed to the published version of the manuscript.

Funding: This material is based upon work supported by the U.S. Department of Energy, Vehicle Technologies Office under Award Number DE-EE0008468.

Data Availability Statement: Vehicle and infrastructure data used in this study can be downloaded from: https://gitlab.com/airabino/opendata (accessed on 6 September 2021).

Conflicts of Interest: The funders had no role in the design of the study; in the collection, analyses, or interpretation of data; in the writing of the manuscript, or in the decision to publish the results.

References

1. *Other Air Pollution from Transportation*; US Environmental Protection Agency: Washington, DC, USA, 2015.
2. International Energy Agency. *CO2 Emissions from Fuel Combustion*; International Energy Agency: Paris, France, 2016.
3. World Health Organization. *World Health Statistics 2016: Monitoring HealthUS6809429B1 for the SDGs Sustainable Development Goals*; World Health Organization: Geneva, Switzerland, 2016.
4. Atabani, A.E.; Badruddin, I.A.; Mekhilef, S.; Silitonga, A.S. A review on global fuel economy standards, labels and technologies in the transportation sector.https://saemobilus.sae.org/content/2011-01-0892/ *Renew. Sustain. Energy Rev.* **2011**, *15*, 4586–4610. [CrossRef]
5. Martinez, C.M.; Hu, X.; Cao, D.; Velenis, E.; Gao, B.; Wellers, M. Energy Management in Plug-in Hybrid Electric Vehicles: Recent Progress and a Connected Vehicles Perspective. *IEEE Trans. Veh. Technol.* **2017**, *66*, 4534–4549. [CrossRef]
6. Uebel, S.; Murgovski, N.; Tempelhahn, C.; Bäker, B. Optimal Energy Management and Velocity Control of Hybrid Electric Vehicles. *IEEE Trans. Veh. Technol.* **2018**, *67*, 327–337. [CrossRef]
7. Luo, Y.; Chen, T.; Li, K. Multi-objective decoupling algorithm for active distance control of intelligent hybrid electric vehicle. *Mech. Syst. Signal Process.* **2015**, *64–65*, 29–45. [CrossRef]
8. Luo, Y.; Chen, T.; Zhang, S.; Li, K. Intelligent Hybrid Electric Vehicle ACC With Coordinated Control of Tracking Ability, Fuel Economy, and Ride Comfort. *IEEE Trans. Intell. Transp. Syst.* **2015**, *16*, 2303–2308. [CrossRef]
9. Wang, Q.; Ayalew, B. A Probabilistic Framework for Tracking the Formation and Evolution of Multi-Vehicle Groups in Public Traffic in the Presence of Observation Uncertainties. *IEEE Trans. Intell. Transp. Syst.* **2018**, *19*, 560–571. [CrossRef]
10. Lin, C.C.; Kang, J.M.; Grizzle, J.; Peng, H. Energy management strategy for a parallel hybrid electric truck. In Proceedings of the 2001 American Control Conference. (Cat. No.01CH37148), Arlington, VA, USA, 25–27 June 2001, Volume 4, pp. 2878–2883. [CrossRef]
11. Serrao, L.; Onori, S.; Rizzoni, G. ECMS as a realization of Pontryagin's minimum principle for HEV control. In Proceedings of the 2009 American Control Conference, St Louis, MO, USA, 10–12 June 2009; pp. 3964–3969. [CrossRef]
12. Asher, Z.D.; Trinko, D.A.; Payne, J.D.; Geller, B.M.; Bradley, T.H. Real-Time Implementation of Optimal Energy Management in Hybrid Electric Vehicles: Globally Optimal Control of Acceleration Events. *J. Dyn. Syst. Meas. Control* **2020**, *142*. [CrossRef]
13. Wu, J.; Ruan, J.; Zhang, N.; Walker, P.D. An Optimized Real-Time Energy Management Strategy for the Power-Split Hybrid Electric Vehicles. *IEEE Trans. Control Syst. Technol.* **2019**, *27*, 1194–1202. [CrossRef]
14. Liang, C.; Xu, X.; Wang, F.; Zhou, Z. Coordinated control strategy for mode transition of dm-phev based on mld. *Nonlinear Dyn.* **2021**, *103*, 809–832. [CrossRef]

15. Tunnell, J.A.; Asher, Z.D.; Pasricha, S.; Bradley, T.H. Towards Improving Vehicle Fuel Economy with ADAS. In *SAE Technical Paper Series*; SAE International: Warrendale, PA, USA, 2018; doi:10.4271/2018-01-0593. [CrossRef]
16. Asher, Z.D.; Patil, A.A.; Wifvat, V.T.; Frank, A.A.; Samuelsen, S.; Bradley, T.H. Identification and Review of the Research Gaps Preventing a Realization of Optimal Energy Management Strategies in Vehicles. *SAE Int. J. Altern. Powertrains* **2019**, *8*. [CrossRef]
17. Baker, D.; Asher, Z.; Bradley, T. Investigation of Vehicle Speed Prediction from Neural Network Fit of Real World Driving Data for Improved Engine On/Off Control of the EcoCAR3 Hybrid Camaro. In *SAE Technical Paper Series*; SAE International: Warrendale, PA, USA, 2017; doi:10.4271/2017-01-1262. [CrossRef]
18. Trinko, D.A.; Asher, Z.D.; Bradley, T.H. Application of Pre-Computed Acceleration Event Control to Improve Fuel Economy in Hybrid Electric Vehicles. In *SAE Technical Paper Series*; SAE International: Warrendale, PA, USA, 2018; doi:10.4271/2018-01-0997. [CrossRef]
19. Bender, F.A.; Kaszynski, M.; Sawodny, O. Drive Cycle Prediction and Energy Management Optimization for Hybrid Hydraulic Vehicles. *IEEE Trans. Veh. Technol.* **2013**, *62*, 3581–3592. [CrossRef]
20. Donateo, T.; Pacella, D.; Laforgia, D. *Development of an Energy Management Strategy for Hybrid Electric Vehicle Based on the Prediction of the Future Driving Cycles by ICT Technologies and Optimized Maps*; SAE Technical Paper; SAE International: Warrendale, PA, USA, 2011.
21. Sun, C.; Moura, S.J.; Hu, X.; Hedrick, J.K.; Sun, F. Dynamic Traffic Feedback Data Enabled Energy Management in Plug-in Hybrid Electric Vehicles. *IEEE Trans. Control Syst. Technol.* **2015**, *23*, 1075–1086.
22. Sun, C.; Hu, X.; Moura, S.J.; Sun, F. Velocity Predictors for Predictive Energy Management in Hybrid Electric Vehicles. *IEEE Trans. Control Syst. Technol.* **2015**, *23*, 1197–1204.
23. Gong, Q.; Li, Y.; Peng, Z. Power management of plug-in hybrid electric vehicles using neural network based trip modeling. In Proceedings of the 2009 American Control Conference, St. Louis, MO, USA, 10–12 June 2009; pp. 4601–4606.
24. Rezaei, A.; Burl, J.B. Prediction of Vehicle Velocity for Model Predictive Control. *IFAC-PapersOnLine* **2015**, *48*, 257–262. [CrossRef]
25. Mohd Zulkefli, M.A.; Zheng, J.; Sun, Z.; Liu, H.X. Hybrid powertrain optimization with trajectory prediction based on inter-vehicle-communication and vehicle-infrastructure-integration. *Transp. Res. Part C Emerg. Technol.* **2014**, *45*, 41–63. [CrossRef]
26. Gaikwad, T.D.; Asher, Z.D.; Liu, K.; Huang, M.; Kolmanovsky, I. *Vehicle Velocity Prediction and Energy Management Strategy Part 2: Integration of Machine Learning Vehicle Velocity PredictionUS6809429B1 with Optimal Energy Management to Improve Fuel Economy*; Technical Report; SAE International: Warrendale, PA, USA, 2019.
27. Gaikwad, T.; Rabinowitz, A.; Motallebiaraghi, F.; Bradley, T.; Asher, Z.; Hanson, L.; Fong, A. *Vehicle Velocity Prediction Using Artificial Neural Network and Effect of Real World Signals on Prediction Window*. Technical Report, SAE International: Warrendale, PA, USA, SAE Technical Paper, 2020.
28. Gong, Q.; Li, Y.; Peng, Z.R. Trip-Based Optimal Power Management of Plug-in Hybrid Electric Vehicles. *IEEE Trans. Veh. Technol.* **2008**, *57*, 3393–3401. [CrossRef]
29. Asher, Z.D.; Tunnell, J.A.; Baker, D.A.; Fitzgerald, R.J.; Farnoush, B.K.; Pasricha, S.; Bradley, T.H. *Enabling Prediction for Optimal Fuel Economy Vehicle Control*; SAE Technical Paper; SAE International: Warrendale, PA, USA, 2018.
30. Baker, D.; Asher, Z.D.; Bradley, T. V2V Communication Based Real-World Velocity Predictions for Improved HEV Fuel Economy. In *SAE Technical Paper Series*; SAE International: Warrendale, PA, USA, 2018; doi:10.4271/2018-01-1000. [CrossRef]
31. Qi, X.; Luo, Y.; Wu, G.; Boriboonsomsin, K.; Barth, M. Deep reinforcement learning enabled self-learning cUS6809429B1ontrol for energy efficient driving. *Transp. Res. Part C Emerg. Technol.* **2019**, *99*, 67–81. [CrossRef]
32. Liu, K.; Asher, Z.; Gong, X.; Huang, M.; Kolmanovsky, I. *Vehicle Velocity Prediction and Energy Management Strategy Part 1: Deterministic and Stochastic Vehicle Velocity Prediction Using Machine Learning*; SAE Technical Paper; SAE International: Warrendale, PA, USA, 2019.
33. Rabinowitz, A.I.; Gaikwad, T.; White, S.; Bradley, T.; Asher, Z. *Infrastructure Data Streams for Automotive Machine Learning Algorithms Research*; Technical Report; SAE Technical Paper; SAE International: Warrendale, PA, USA, 2020.
34. Frank, A.A. Control Method and Apparatus for Internal Combustion Engine Electric Hybrid Vehicles. US6809429B1, 26 October 2004.
35. Amini, M.R.; Hu, Q.; Wang, H.; Feng, Y.; Kolmanovsky, I.; Sun, J. Experimental validation of eco-driving and eco-heating strategies for connected and automated hevs. In *SAE Technical Paper Series*; SAE International: Warrendale, PA, USA, 2021. [CrossRef]
36. Gong, X.; Wang, J.; Ma, B.; Lu, L.; Hu, Y.; Chen, H. Real-time integrated power and thermal management of connected hevs based on hierarchical model predictive control. *IEEE/ASME Trans. Mechatron.* **2021**, *26*, 1271–1282. US6809429B1 [CrossRef]
37. Wang, H.; Amini, M.R.; Hu, Q.; Kolmanovsky, I.; Sun, J. Eco-Cooling control strategy for Automotive Air-Conditioning System: Design and experimental validation. *IEEE Trans. Control Syst. Technol.* **2020**, 1–12. [CrossRef]
38. J2735: Dedicated Short Range Communications (DSRC) Message Set Dictionary™-SAE International. Available online: https://www.sae.org/standards/content/j2735_200911/ (accessed on 14 June 2021).
39. J3016: Taxonomy and Definitions for Terms Related to Driving Automation Systems for On-Road Motor Vehicles™-SAE International. Available online: https://www.sae.org/standards/content/j3016_201806/ (accessed on 14 June 2021).
40. Ryosuke Okuda, Y.K.; Terashima, K. A survey of technical trend of ADAS and autonomous driving. In Proceedings of the Technical Program—2014 International Symposium on VLSI Technology, Systems and Application (VLSI-TSA), Hsinchu, Taiwan, 28–30 April 2014.

41. Gschwendtner, C.; Sinsel, S.R.; Stephan, A. Vehicle-to-X (V2X) implementation: An overview of predominate trial configurations and technical, social and regulatory challenges. *Renew. Sustain. Energy Rev.* **2021**, *145*, 110977. j.rser.2021.110977. [CrossRef]
42. Musardo, C.; Rizzoni, G.; Guezennec, Y.; Staccia, B. A-ECMS: An Adaptive Algorithm for Hybrid Electric Vehicle Energy Management. *Eur. J. Control* **2005**, *11*, 509–524.: 10.3166/ejc.11.509-524. [CrossRef]
43. Sun, C.; He, H.; Sun, F. The Role of Velocity Forecasting in Adaptive-ECMS for Hybrid Electric Vehicles. *Energy Procedia* **2015**, *75*, 1907–1912. [CrossRef]
44. Asher, Z.D.; Baker, D.A.; Bradley, T.H. Prediction error applied to hybrid electric vehicle optimal fuel economy. *IEEE Trans. Control Syst. Technol.* **2017**, 26, 2121–2134. [CrossRef]
45. Shi, W.; Alawieh, M.B.; Li, X.; Yu, H. Algorithm and hardware implementation for visual perception system in autonomous vehicle: A survey. *Integration* **2017**, *59*, 148–156. [CrossRef]
46. Onori, S.; Serrao, L.; Rizzoni, G. *Hybrid Electric Vehicles: Energy Management Strategies*; Springer: London, UK, 2016.
47. SAE International Kirk, D.E. *Optimal Control Theory: An Introduction*; Courier Corporation: Chelmsford, MA, USA, 2004.
48. Huang, M.; Zhang, S.; Shibaike, Y. *Real-time Long Horizon Model Predictive Control of a Plug-in Hybrid Vehicle Power-Split Utilizing Trip Preview*; Technical Report; SAE Technical Paper; SAE International: Warrendale, PA, USA, 2019.
49. Meyer, R.T.; DeCarlo, R.A.; Meckl, P.H.; Doktorcik, C.; Pekarek, S. Hybrid Model Predictive Power Management of A Fuel Cell-Battery Vehicle. *Asian J. Control* **2013**, *15*, 363–379. [CrossRef]
50. Kim, N.; Rousseau, A.; Rask, E. Autonomie Model Validation with Test Data for 2010 Toyota Prius. In *SAE Technical Paper Series*; SAE International: Warrendale, PA, USA, 2012. [CrossRef]
51. Downloadable Dynamometer Database: Argonne National Laboratory. Available online: https://www.anl.gov/es/downloadable-dynamometer-database (accessed on 17 March 2021).
52. Hochreiter, S.; Schmidhuber, J. Long short-term memory. *Neural Comput.* **1997**, *9*, 1735–1780. [CrossRef]
53. Olah, C. Understanding Lstm Networks. Available online: https://colah.github.io/posts/2015-08-Understanding-LSTMs/ (accessed on 4 May 2021)
54. Huang, C.J.; Kuo, P.H. A Deep CNN-LSTM Model for Particulate Matter (PM2.5) Forecasting in Smart Cities. *Sensors* **2018**, *18*, 2220. [CrossRef] [PubMed]
55. Nicholson, C. A Beginner's Guide to LSTMs and Recurrent Neural Networks. Available online: https://pathmind.com/wiki/lstm (accessed on 6 May 2021).